sustainability

Article

Research on Excavator Trajectory Control Based on Hybrid Interpolation

Jing Yang [1,2,3], Yingjie Gao [1,2,3,*], Rui Guo [1,2,3], Qingshan Gao [1,2,3] and Jingyi Zhao [1,2,3]

1 Hebei Provincial Key Laboratory of Heavy Machinery Fluid Power Transmission and Control, Yanshan University, Qinhuangdao 066004, China
2 Key Laboratory of Advanced Forging & Stamping Technology and Science, Yanshan University, Qinhuangdao 066004, China
3 Hebei Key Laboratory of Special Delivery Equipment, Yanshan University, Qinhuangdao 066004, China
* Correspondence: yjgao@ysu.edu.cn

Abstract: In this study, to address the issues of tooth tip operation discontinuity and jitter during autonomous excavator operation, a multi-segment mixed interpolation method utilizing different higher-order polynomials has been proposed. This approach is designed to optimize the tooth tip trajectory of the excavator under multiple constraints, resulting in a smoother trajectory. Specifically, the single-bucket excavator was chosen as the research object, and three different high-order mixed polynomials were utilized to interpolate the trajectory of the digging discrete points. Through a comparative analysis under multiple constraints, this study explored and analyzed the joint angle, angular velocity, and angular acceleration curves of each excavator's joint. An experimental platform was established to investigate the hydraulic system of an excavator, and the optimal trajectory was controlled using a high-order mixed polynomial interpolation. The results of this study demonstrate that the tracking accuracy of the excavator's actuator under the optimal interpolation strategy is high, with a maximum displacement deviation of ±3 mm. Additionally, during operation, the excavator manipulator runs smoothly and continuously with minimal flexible impact and vibration.

Keywords: hydraulic excavator; higher-order polynomial; mixed interpolation strategy; trajectory planning

check for updates

Citation: Yang, J.; Gao, Y.; Guo, R.; Gao, Q.; Zhao, J. Research on Excavator Trajectory Control Based on Hybrid Interpolation. *Sustainability* **2023**, *15*, 6761. https://doi.org/10.3390/su15086761

Academic Editors: Paris Fokaides, Mingwei Sun, Jin Tao, Hao Sun and Qinglin Sun

Received: 10 March 2023
Revised: 10 April 2023
Accepted: 13 April 2023
Published: 17 April 2023

1. Introduction

The market demand and sales of excavators in construction machinery have increased with the continuous development of various national economic sectors and military engineering. According to the China Construction Machinery Industry Association, total excavator sales in 2020 were 327,605, up 39% annually. Total annual sales of domestic excavators increased by 40.1%, reaching 292,864; total annual sales of export excavators was 34,741, up 30.5% annually. Excavators are important construction machinery that reduce heavy physical labor, improving labor productivity, accelerating construction speed, ensuring project quality, and reducing costs. In complex environmental conditions, excavators can complete numerous tasks including flat slopes underwater operations, pipeline operations, precision digging, and airport rectification. However, the diversification of excavator use, operation accuracy, and standardization of operation technology, as well as how to improve the intelligent technology of excavators are the major challenges in the research and design of construction machinery.

The research on excavator intelligent technology can be broadly classified into four main categories, namely machine perception, network communication, fault diagnosis, and intelligent trajectory control [1,2]. In terms of machine perception, a three-dimensional local terrain model for the excavation target was created through the fusion of multiple sensor technologies and stereo camera detection and tracking technology. This enables the excavator to achieve autonomous excavation control [3–6]. In the domain of network communication, Quang et al. [7] have proposed a method to improve the working efficiency of the operator by replacing the traditional display with a head-mounted display (HMD) and combining it with head tracking and monitoring techniques. This helps to address the blind areas of the excavator operator's vision. Li et al. [8] have proposed a fault diagnosis method for hydraulic excavators that combines a fault tree and fuzzy neural network. This approach was based on monitoring data of the working state of hydraulic excavators as samples, considering the decentralized and weak failure features of hydraulic excavators. In another study, Li et al. [9] proposed an approach that combines fault trees with expert system rules to achieve fault diagnosis of hydraulic excavators. The goal of intelligent trajectory control of the excavator is to achieve operational automation, thereby improving and enhancing its working efficiency, shortening the cycle period, reducing energy consumption, prolonging the service span of the machine, improving working conditions, and reducing the labor intensity of operators. Therefore, the accuracy of automatic excavation is highly dependent on the quality of trajectory control. A nonlinear constraint problem has been suggested by several researchers, where time optimization, minimum energy, and minimum torque are the objectives, while speed and acceleration are the constraints. The optimization of the target trajectory was achieved by combining various interpolation strategies, ensuring the continuity of angular velocity and angular acceleration of the mining trajectory, leading to improved efficiency and reduced energy consumption of the mining action [10–15]. The B-spline curve was used to interpolate the autonomous planning trajectory of the excavator. By utilizing joint angular velocity, angular acceleration, and acceleration as constraints, the dynamic trajectory planning method of the excavator was improved through the application of fuzzy logic control. This method ensures high efficiency and smoothness during the excavation process, as evidenced by previous works [16–21]. In order to achieve a continuous mining trajectory, a multi-objective optimization trajectory was established, considering driving limits and geometric conditions. The paper then utilized different optimization algorithms to optimize the target trajectory, leading to an improvement in tracking accuracy of the mining trajectory, which has been demonstrated in prior studies [22–25]. To construct a multi-segment interpolation mining trajectory, this study utilized a polynomial interpolation combination. They optimized the objective function by employing an optimization algorithm, taking into account the change in velocity and acceleration as constraints, to achieve a continuous and smooth mining trajectory [26,27]. In order to address the issue of vibration resulting from flexible impact during the excavation trajectory process, which can negatively affect the operator, several researchers have studied the vibration and impact phenomena in the excavation process. Through the establishment of various models and control strategies, the impact generated during the excavation process was reduced, thereby improving the operator's driving comfort. Previous works have contributed to this effort [28–33].

Various types of interpolation curves were employed for planning the trajectory of excavators. The B-spline interpolation curve order augmentation can be used to minimize the angular velocity of the trajectory, but it has some constraints. Non-uniform rational B-spline curve order augmentation results in an increase in the complexity of its solution. The increase in polynomial interpolation order guarantees the continuity of trajectory operation. This paper proposes a trajectory planning method for an excavator based on a piecewise combination of high-order polynomial interpolation, which was grounded on the kinematics model, polynomial interpolation technology, and hydraulic control system of a single-bucket excavator. The proposed method aims to ensure continuity of velocity and acceleration during the operation of tooth tip trajectory. Therefore, the primary contributions of this paper encompass:

(1) The research object of this paper is the structure of the single-bucket excavator test bench. To achieve continuity of angular acceleration rate in the excavation trajectory, this paper establishes a kinematics model and introduces high-order polynomial interpolation.

(2) This paper proposes to interpolate various combinations of cubic, quartic, quintic, and seventh-order polynomials. The angle, angular velocity, and angular acceleration of the trajectory operation were compared to select the optimal combination method for optimizing the digging trajectory.

(3) The mapping relationship of the kinematic model was used to convert each joint angle variable into the corresponding actuator displacement variable after trajectory optimization. To verify the reliability of trajectory planning and tracking control, the optimized trajectory was controlled through the experimental platform of the excavator.

This paper is structured as follows: Section 2 aims to establish the kinematics modeling of a single-bucket excavator, serving as a theoretical basis for trajectory planning. Subsequently, Section 3 excavates the target trajectory and employs interpolation strategy for trajectory planning. In Section 4, a rigorous selection process of optimal multi-segment hybrid interpolation combination is undertaken to ensure the trajectory tracking experiment's precision. Finally, the effectiveness of the proposed interpolation strategy is comprehensively validated and summarized in Section 5.

2. Kinematic Modeling of Excavator

Figure 1 illustrates the structure of the single-bucket excavator test platform, encompassing the boom, arm, bucket, and base. Anchor bolts secured the base to the ground, and a hydraulic control valve group was positioned on the base platform. The boom was hinged to the base via the pin shaft; the arm was connected with the boom through the pin shaft; the bucket was attached to the arm through the pin shaft. A displacement sensor was installed on the hydraulic actuator of the excavator to detect its displacement. Real-time dynamic adjustment was conducted in accordance with the target displacement and the detected displacement, thus accomplishing the displacement closed-loop control of the excavator's hydraulic actuator.

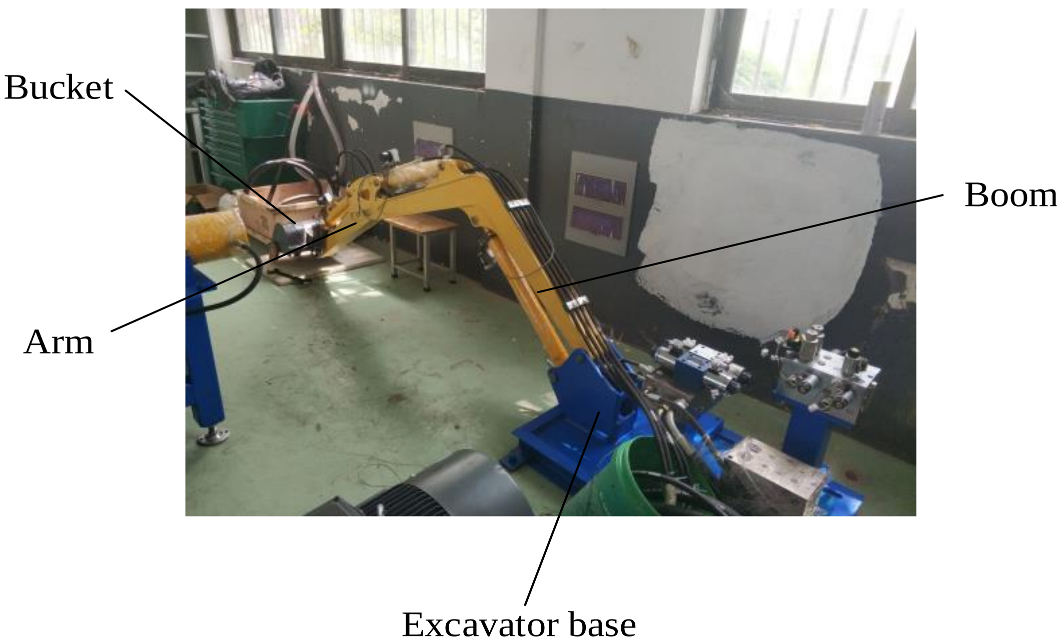

Figure 1. Structure of single-bucket excavator test platform.

2.1. Forward Kinematics

The boom of the single-bucket excavator test platform resembled a three degree of freedom linkage mechanism based on the D-H parameter coordinate method. The origin of the base coordinate system for the test platform was the hinge point between the base and the boom, and the corresponding coordinate system for each joint was established sequentially, with the Z-axis representing collinearity with the joint axis. Figure 2 exhibits the coordinate system for each joint.

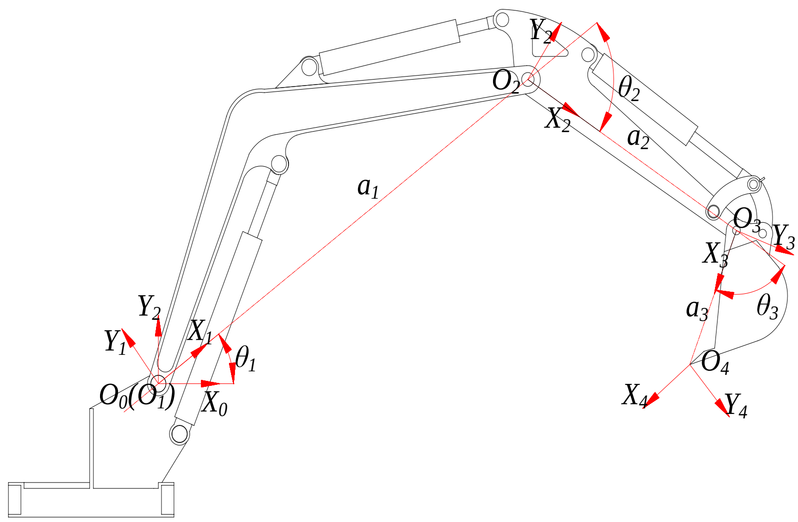

Figure 2. Coordinate system of each joint of excavator.

The D-H parameters of each joint were obtained from the joint coordinate system and the connecting rod parameters were established in Figure 2 (Table 1).

Table 1. D-H parameters of excavator manipulator.

Joint i	α_i	l_i	d_i	Variable θ_i	Value Range of Variables
1	0°	1473 mm	0	θ_1	[−4°, 67°]
2	0°	797 mm	0	θ_2	[−165°, −39°]
3	0°	414 mm	0	θ_3	[−65°, 24°]

According to the base coordinate system and D-H parameter table established by the excavator manipulator, the pose matrix of the excavator bucket end relative to the base coordinate system can be solved by the transformation matrix between the adjacent joint coordinate systems of the manipulator.

$$M_{03} = M_{01}M_{12}M_{23} = \begin{bmatrix} c\theta_{123} & -s\theta_{123} & 0 & l_1 * c\theta_1 + l_2 * c\theta_{12} + l_3 * c\theta_{123} \\ s\theta_{123} & -c\theta_{123} & 0 & l_1 * s\theta_1 + l_2 * s\theta_{12} + l_3 * s\theta_{123} \\ 0 & 0 & 1 & 0 \\ 0 & 0 & 0 & 1 \end{bmatrix} \tag{1}$$

In Formula (1):

$$\begin{array}{l} s\theta_i = \sin(\theta_i)\ s\theta_{ij} = \sin(\theta_i + \theta_j)\ s\theta_{ijk} = \sin(\theta_i + \theta_j + \theta_k) \\ c\theta_i = \cos(\theta_i)\ c\theta_{ij} = \cos(\theta_i + \theta_j)\ c\theta_{ijk} = \cos(\theta_i + \theta_j + \theta_k) \end{array} \tag{2}$$

From the pose matrix of Equation (1), the 3-D space coordinate equation of excavator bucket trajectory can be known:

$$\begin{cases} p_x = l_1 * c\theta_1 + l_2 * c\theta_{12} + l_3 * c\theta_{123} \\ p_y = l_1 * s\theta_1 + l_2 * s\theta_{12} + l_3 * s\theta_{123} \\ p_z = 0 \end{cases} \tag{3}$$

2.2. Inverse Kinematics

Additionally, the bucket end pose could be resolved through forward kinematics analysis of the excavator manipulator. The angle variables for each joint of the manipulator could be solved reversibly via the end pose, forming a crucial foundation for trajectory planning. Nevertheless, the inverse kinematics solution was relatively intricate, and the solution process entailed nonlinear problems, potentially yielding no solution or multiple solutions simultaneously. Considering the three-degree-of-freedom distinction of the excavator manipulator structure, the geometric method was employed to execute the inverse kinematics solution process, which was straightforward. Figure 2 displays the set space coordinate at coordinate system O_3 as $(O_{3x}, O_{3y}, 0)$, and the space coordinate at coordinate system O_4 as $(O_{4x}, O_{4y}, 0)$. The inverse kinematics solution for the excavator manipulator is:

$$\begin{cases} \theta_1 = \arccos(\frac{(O_{3x}^2+O_{3y}^2)+a_1^2-a_2^2}{2a_1\sqrt{O_{3x}^2+O_{3y}^2}}) + \arctan(\frac{O_{3y}}{O_{3x}}) \\ \theta_2 = \arccos(\frac{a_1^2+a_2^2-(O_{3x}^2+O_{3y}^2)}{2a_1a_1}) - \pi \\ \theta_3 = \arccos(\frac{a_2^2+(O_{3x}^2+O_{3y}^2)-a_1^2}{2a_2\sqrt{O_{3x}^2+O_{3y}^2}}) + \arccos(\frac{a_3^2+(O_{3x}^2+O_{3y}^2)-(O_{4x}^2+O_{4y}^2)}{2a_3\sqrt{O_{3x}^2+O_{3y}^2}}) - \pi \end{cases} \tag{4}$$

2.3. Mapping of Drive Space and Joint Space

The hydraulic actuators of the single-bucket excavator test platform comprised a boom cylinder, arm cylinder, and bucket cylinder. The angle variables of each joint established a mapping relationship via the geometric model of the excavator and the telescopic displacement of the hydraulic cylinder. By analyzing the geometric dimensions of the excavator, the mapping relationship between the drive space and the joint space was devised, and the displacement parameters were converted into the joint angle parameters to accomplish the trajectory planning for the excavator. Figure 3 unveils the geometric dimensions of the excavator's arm.

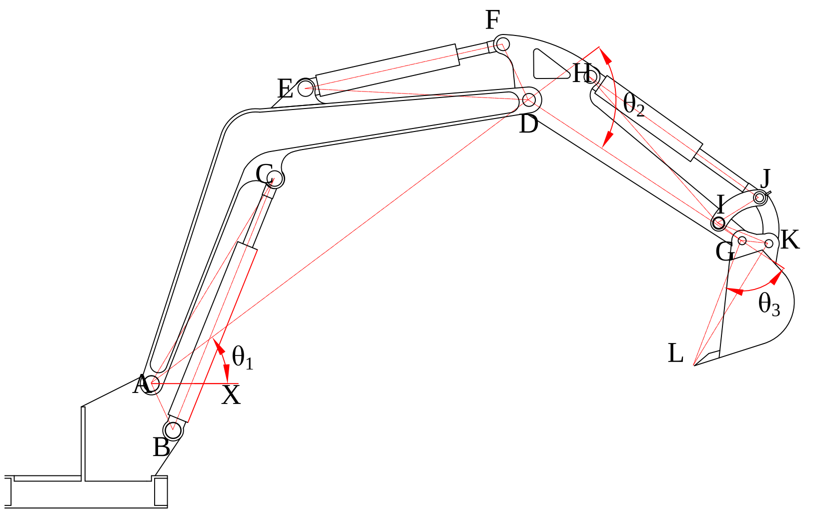

Figure 3. Geometric dimensions of excavator's arm.

According to the geometric relationship between the arm and the bucket mechanism (Figure 3):

$$\angle BAC = \angle BAX + \theta_1 + \angle CAD \tag{5}$$

$$\begin{cases} L_{BC} = \sqrt{L_{AB}^2 + L_{AC}^2 - 2L_{AB}L_{AC}\cos(\theta_1 + \angle BAX + \angle CAD)} \\ \theta_1 = \arccos\frac{L_{AB}^2+L_{AC}^2-L_{BC}^2}{2L_{AB}L_{AC}} - \angle BAX - \angle CAD \end{cases} \tag{6}$$

According to the geometric relationship between the boom and the arm mechanism:

$$\angle EDF = \pi - \angle ADE - \theta_2 - \angle FDG \tag{7}$$

$$\begin{cases} L_{EF} = \sqrt{L_{DE}^2 + L_{DF}^2 - 2L_{DE}L_{DF}\cos(\pi - \theta_2 - \angle ADE - \angle FDG)} \\ \quad\;\; = \sqrt{L_{DE}^2 + L_{DF}^2 + 2L_{DE}L_{DF}\cos(\theta_2 + \angle ADE + \angle FDG)} \\ \theta_2 = \arccos\frac{L_{DE}^2 + L_{DF}^2 - L_{EF}^2}{-2L_{DE}L_{DF}} - \angle ADE - \angle FDG \end{cases} \quad (8)$$

According to the geometric relationship between the arm and the bucket mechanism:

$$\angle HIJ = \arccos\frac{L_{HI}^2 + L_{IJ}^2 - L_{HJ}^2}{2L_{HI}L_{IJ}} \quad (9)$$

$$\angle HIJ = \angle HIG - \angle JIG \quad (10)$$

$$\begin{cases} L_{JG} = \sqrt{L_{JI}^2 + L_{IG}^2 - 2L_{JI}L_{IG}\cos\angle JIG} \\ \angle IGJ = \arccos\frac{L_{GI}^2 + L_{JG}^2 - L_{IJ}^2}{2L_{IG}L_{JG}} \end{cases} \quad (11)$$

$$\angle JGK = \arccos\frac{L_{JG}^2 + L_{GK}^2 - L_{JK}^2}{2L_{JG}L_{GK}} \quad (12)$$

$$\begin{aligned} \theta_3 \quad &= \pi - \angle IGD - \angle LGK - \angle JGK - \angle IGJ \\ &= \pi - \angle IGD - \angle LGK \\ &- \arccos\frac{L_{JI}^2 + L_{IG}^2 - 2L_{JI}L_{IG}\cos(\angle HIG - \arccos\frac{L_{HI}^2 + L_{IJ}^2 - L_{HJ}^2}{2L_{HI}L_{IJ}}) + L_{GK}^2 - L_{JK}^2}{2\sqrt{L_{JI}^2 + L_{IG}^2 - 2L_{JI}L_{IG}\cos(\angle HIG - \arccos\frac{L_{HI}^2 + L_{IJ}^2 - L_{HJ}^2}{2L_{HI}L_{IJ}})}\,L_{GK}} \\ &- \arccos\frac{2L_{IG}^2 - 2L_{JI}L_{IG}\cos(\angle HIG - \arccos\frac{L_{HI}^2 + L_{IJ}^2 - L_{HJ}^2}{2L_{HI}L_{IJ}})}{2\sqrt{L_{JI}^2 + L_{IG}^2 - 2L_{JI}L_{IG}\cos(\angle HIG - \arccos\frac{L_{HI}^2 + L_{IJ}^2 - L_{HJ}^2}{2L_{HI}L_{IJ}})}\,L_{IG}} \end{aligned} \quad (13)$$

Substituting the size parameters of the boom, arm, and bucket of the single-bucket excavator and the stroke data of the hydraulic cylinder into the Formulas (6), (8), and (9), ensures the establishment of the relationship between the change in each joint angle variable and the displacement variable of the hydraulic cylinder.

Figure 4 shows that the displacement of the boom cylinder continuously increases when the joint angle between the excavator base and the boom increases continuously; When the joint angle between the boom and the arm decreases, the displacement of the arm cylinder increases; When the joint angle between the arm and the bucket decreases, the displacement of the bucket cylinder increases.

2.4. Workspace Analysis

The end operation space of the excavator bucket is a collection of all position points that indicate the work of the bucket tooth in this space. The analysis of its workspace reflects the flexibility and agility of the excavator manipulator, providing theoretical guidance for the obstacle dismissal of the bucket tooth during the excavation process.

The Monte Carlo algorithm was used to solve the space of the bucket end trajectory. The principle adopts the forward kinematics solution to compute the pose space of the end of the excavator relative to the base coordinate system. By combining the extreme value theory with the optimization theory, the range of each joint variable in the D-H parameter table is discretized to set the position space points that the tooth tip trajectory can reach, hence solving the excavator workspace.

Figure 5 show a similar working space at the end of the bucket of the single-bucket excavator test platform to the half-moon shape. The shape of the bucket end on the X-Y working plane reveals that the maximum excavation height of the single-bucket excavator test platform is 1.8 m, the maximum excavation radius is 2.7 m, and the maximum excavation depth is 1.3 m. The working space parameters of the excavator are consistent with the given mining parameters, hence confirming the reliability of the kinematics model.

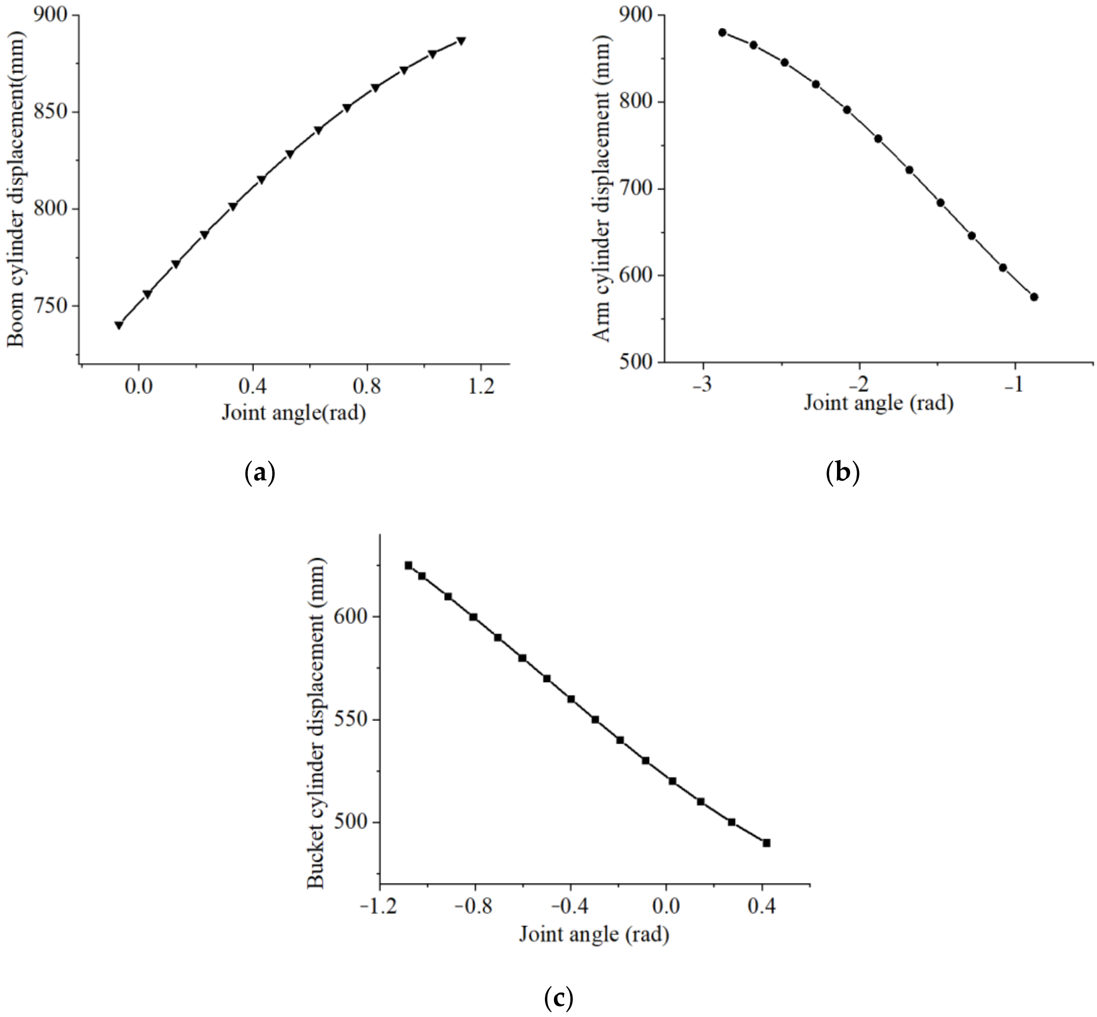

Figure 4. Relationship between hydraulic actuator and joint variable of excavator: (**a**) Boom (**b**) Arm (**c**) Bucket.

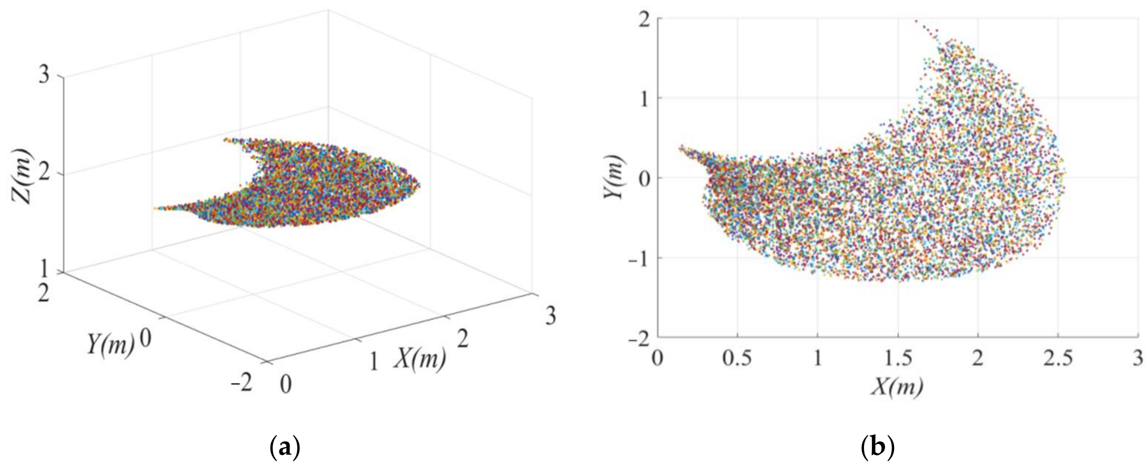

Figure 5. Working space: (**a**) working space at the end of excavator bucket; (**b**) X-Y working plane at bucket end of excavator.

3. Excavating Trajectory Planning

Investigation into the intelligent control of hydraulic excavators seeks to enhance the semi-automatic or automatic operation capacity of hydraulic excavators, render them intelligent, alleviate the labor intensity of operators, and finally boost operation efficiency. Trajectory planning and control strategy constitute the pivotal technology for semi-automatic or automatic operation of the hydraulic excavator.

Research on hydraulic excavator trajectory planning concentrates on governing the movement trajectory of the bucket end and determining the movement relationship between the boom, the stick, and the bucket, as well as the movement trajectory equation of the bucket end. Conversely, the motion relationship between the boom, stick, and bucket was inversely addressed when the bucket end trajectory was provided.

The appropriate step size was selected to discretize the operation trajectory, and the pose sequence of the bucket end in Cartesian coordinate space was obtained when any operation trajectory was supplied at the end of the bucket; The angle variables of each joint in the joint space were ascertained using the inverse kinematics of the excavator, and the combined polynomial interpolation technique sought to plan the trajectory of each joint angle parameter. The joint angle function of the optimal combination interpolation was converted into the displacement sequence of each hydraulic cylinder of the excavator. The experimental platform for the excavator hydraulic system was established to control the displacement of each cylinder in a closed loop (Figure 6).

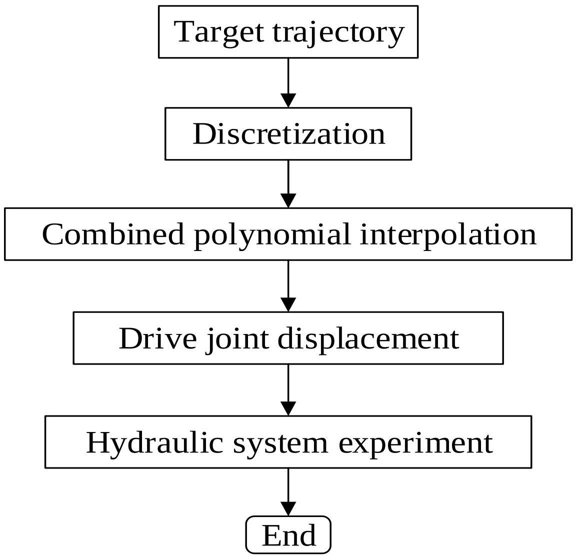

Figure 6. Excavator trajectory planning flow chart.

3.1. Excavating Trajectory Discretization

The space for trajectory planning of the excavator bucket end primarily encompassed: the joint space method and Cartesian space. Each space method necessitated the continuity and smoothness of the planned trajectory to ensure the stability of the excavator actuator. Upon provision of the end target trajectory of the excavator bucket, the key points of trajectory discretization were selected in Cartesian space. Inverse kinematics were employed to solve the joint angle corresponding to the key points before interpolating the discrete joint angle.

As demonstrated in Figure 7, the target trajectory of the end of the excavator bucket was given in the Cartesian coordinate space. The selected target trajectory is the trajectory of the excavator excavation operation, and six key points are selected following the discretization of the target trajectory.

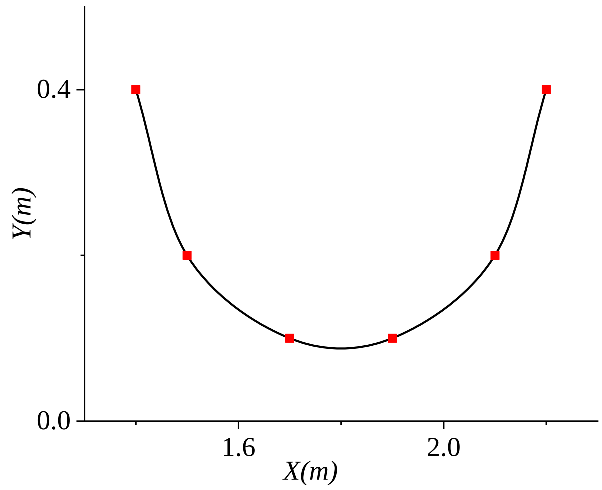

Figure 7. Excavator trajectory.

Based on the six joint points following the discretization of the target trajectory at the end of the bucket, combined with the inverse solution equation of the excavator kinematics, the six groups of discrete key points can be converted from the pose space to the joint space. The results are presented in Table 2.

Table 2. Conversion from configuration space to joint space of trajectory discrete control points.

Pose Point	Boom Joint/(°)	Arm Joint/(°)	Bucket Joint/(°)
(2.2,0.4,0)	34.83	−40.32	−56.16
(2.1,0.2,0)	34.05	−50.52	−57.47
(1.9,0.1,0)	37.27	−65.58	−58.15
(1.7,0.1,0)	41.75	−77.73	−60.14
(1.5,0.2,0)	49.39	−89.13	−60.26
(1.4,0.4,0)	58.46	−92.13	−61.07

3.2. Construction of Mixed Interpolation Function

The excavation path was categorized into five segments by six groups of discrete key points of the bucket end track of the excavator. Besides, three different high-order polynomial combination interpolations (3-4-5-4-3, 3-4-7-4-3, 3-3-7-3-3) were utilized to plan the trajectory of the five sections. For the segmented trajectory, the velocity and acceleration of the starting position were required to be zero, and the joint angle, angular velocity, angular acceleration, and jerk change rate of the remaining connection path points were smooth and continuous for the stability of the hydraulic excavator during operation.

Considering the mapping relationship between the function of each joint angle variable and time, the normalized method was applied to address the time variable dimensionless hence facilitating the solution [27].

$$t = \frac{\tau - \tau_{i-1}}{\tau_i - \tau_{i-1}} \tag{14}$$

In the above formula: $\tau \in [\tau_i\text{-}1, \tau_i]$ represents the time set of each trajectory; τ_{i-1} is the starting time of i terminal trajectory; τ_i is the termination time of i terminal trajectory; t is the dimensionless expression of the time learned by the i terminal trajectory; The trajectory of each joint k (k = 1, 2, 3) of the excavator is represented by the sequence formed by the combination interpolation of polynomial $h_i(t)$(I = 1, 2, 3, 4, 5).

Polynomial interpolation expression of any joint variable in the excavator joint space was set as 3-4-5-4-3.

$$\begin{cases} h_1(t) = a_{13}t^3 + a_{12}t^2 + a_{11}t + a_{10} \\ h_2(t) = a_{24}t^4 + a_{23}t^3 + a_{22}t^2 + a_{21}t + a_{20} \\ h_3(t) = a_{35}t^5 + a_{34}t^4 + a_{33}t^3 + a_{32}t^2 + a_{31}t + a_{30} \\ h_4(t) = a_{44}t^4 + a_{43}t^3 + a_{42}t^2 + a_{41}t + a_{40} \\ h_5(t) = a_{53}t^3 + a_{52}t^2 + a_{51}t + a_{50} \end{cases} \tag{15}$$

According to the above Formula (15), the actual time variable τ, the expressions of velocity, acceleration, and jerk of the polynomial interpolation trajectory in the i segment can be obtained by calculating the first, second, and third derivatives as follows:

$$\begin{cases} v_i(t) = \frac{dh_i(t)}{d\tau} = \frac{dh_i(t)}{dt} * \frac{dt}{d\tau} = \frac{\dot{h}_i(t)}{t_i} \\ a_i(t) = \frac{d^2h_i(t)}{d\tau^2} = \frac{d\ddot{h}_i(t)}{t_i^2} \\ \dot{a}_i(t) = \frac{da_i(t)}{d\tau} = \frac{d^3h_i(t)}{d\tau^3} = \frac{d\dddot{h}_i(t)}{t_i^3} \end{cases} \tag{16}$$

The continuity of the starting point, angular velocity, angular acceleration, and jerk of each segment of the trajectory is essential for the smoothness of the multi-segment interpolation trajectory.

The smoothness constraint of the excavator trajectory joint angle is:

$$\begin{cases} h_1(0) = \theta_1 \\ h_2(0) = \theta_2 \\ h_3(0) = \theta_3 \\ h_4(0) = \theta_4 \\ h_5(0) = \theta_5 \end{cases} \begin{cases} h_1(t_1) = h_2(0) \\ h_2(t_2) = h_3(0) \\ h_3(t_3) = h_4(0) \\ h_4(t_4) = h_5(0) \\ h_5(t_5) = \theta_6 \end{cases} \tag{17}$$

The smoothness constraint of the angular velocity of the excavator trajectory joint is:

$$\begin{cases} \dot{h}_1(0) = 0 \\ \dot{h}_1(t_1) = \dot{h}_2(0) \\ \dot{h}_2(t_2) = \dot{h}_3(0) \end{cases} \begin{cases} \dot{h}_3(t_3) = \dot{h}_4(0) \\ \dot{h}_4(t_4) = \dot{h}_5(0) \\ \dot{h}_5(t_5) = 0 \end{cases} \tag{18}$$

The smoothness constraint of the angular acceleration of the excavator trajectory joint is:

$$\begin{cases} \ddot{h}_1(0) = 0 \\ \ddot{h}_1(t_1) = \ddot{h}_2(0) \\ \ddot{h}_2(t_2) = \ddot{h}_3(0) \end{cases} \begin{cases} \ddot{h}_3(t_3) = \ddot{h}_4(0) \\ \ddot{h}_4(t_4) = \ddot{h}_5(0) \\ \ddot{h}_5(t_5) = 0 \end{cases} \tag{19}$$

The smoothness constraints of the angular jerk of the excavator trajectory joint is:

$$\begin{cases} \dddot{h}_2(t_2) = \dddot{h}_3(0) \\ \dddot{h}_3(t_3) = \dddot{h}_4(0) \end{cases} \tag{20}$$

According to the smoothness constraints and transition conditions of the excavator trajectory joint operation, the 24-order equation of the polynomial combination interpolation (3-4-5-4-3) of the three joints of the excavator can be determined, and the matrix expressions of the polynomial combination coefficient, interpolation time and discrete angle are formed.

$$Ax = B \tag{21}$$

In the above expression, A represents the matrix that changes with the time of polynomial combination interpolation (3-4-5-4-3), x is the combination coefficient matrix of multiple higher-order polynomial combination interpolation, and B is the interpolation angle matrix of multiple discrete points that the excavator track joint passes through.

$$A = \begin{pmatrix} A_1 & A_2 & 0 & 0 & 0 \\ 0 & A_3 & A_4 & 0 & 0 \\ 0 & 0 & A_5 & A_6 & 0 \\ 0 & 0 & 0 & A_7 & A_8 \\ 0 & 0 & 0 & 0 & A_9 \end{pmatrix} \tag{22}$$

$$x = \begin{bmatrix} x_1 & x_2 & x_3 & x_4 & x_5 \end{bmatrix}^T \tag{23}$$

$$B = \begin{bmatrix} B_1 & B_2 & B_3 & B_4 & B_5 \end{bmatrix}^T \tag{24}$$

In Formulas (22)–(24)

$$A_1 = \begin{bmatrix} t_1^3 & t_1^2 & t_1 & 1 \\ 3t_1^2 & 2t_1 & 1 & 0 \\ 6t_1 & 2 & 0 & 0 \\ 0 & 0 & 0 & 1 \\ 0 & 0 & 1 & 0 \\ 0 & 2 & 0 & 0 \end{bmatrix} \tag{25}$$

$$A_2 = \begin{bmatrix} 0 & 0 & 0 & 0 & -1 \\ 0 & 0 & 0 & -1 & 0 \\ 0 & 0 & -2 & 0 & 0 \\ 0 & 0 & 0 & 0 & 0 \\ 0 & 0 & 0 & 0 & 0 \\ 0 & 0 & 0 & 0 & 0 \end{bmatrix} \tag{26}$$

$$A_3 = \begin{bmatrix} t_2^4 & t_2^3 & t_2^2 & t_2 & 1 \\ 4t_2^3 & 3t_2^2 & 2t_2 & 1 & 0 \\ 12t_2^2 & 6t_2 & 2 & 0 & 0 \\ 24t_2 & 6 & 0 & 0 & 0 \\ 0 & 0 & 0 & 0 & 1 \end{bmatrix} \tag{27}$$

$$A_4 = \begin{bmatrix} 0 & 0 & 0 & 0 & 0 & -1 \\ 0 & 0 & 0 & 0 & -1 & 0 \\ 0 & 0 & 0 & -2 & 0 & 0 \\ 0 & 0 & -6 & 0 & 0 & 0 \\ 0 & 0 & 0 & 0 & 0 & 0 \end{bmatrix} \tag{28}$$

$$A_5 = \begin{bmatrix} t_3^5 & t_3^4 & t_3^3 & t_3^2 & t_3 & 1 \\ 5t_3^4 & 4t_3^3 & 3t_3^2 & 2t_3 & 1 & 0 \\ 20t_3^3 & 12t_3^2 & 6t_3 & 2 & 0 & 0 \\ 60t_3^2 & 24t_3 & 6 & 0 & 0 & 0 \\ 0 & 0 & 0 & 0 & 0 & 1 \end{bmatrix} \tag{29}$$

$$A_6 = \begin{bmatrix} 0 & 0 & 0 & 0 & -1 \\ 0 & 0 & 0 & -1 & 0 \\ 0 & 0 & -2 & 0 & 0 \\ 0 & -6 & 0 & 0 & 0 \\ 0 & 0 & 0 & 0 & 0 \end{bmatrix} \tag{30}$$

$$A_7 = \begin{bmatrix} t_4^4 & t_4^3 & t_4^2 & t_4 & 1 \\ 4t_4^3 & 3t_4^2 & 2t_4 & 1 & 0 \\ 12t_4^2 & 6t_4 & 2 & 0 & 0 \\ 0 & 0 & 0 & 0 & 1 \end{bmatrix} \tag{31}$$

$$A_8 = \begin{bmatrix} 0 & 0 & 0 & -1 \\ 0 & 0 & -1 & 0 \\ 0 & -2 & 0 & 0 \\ 0 & 0 & 0 & 0 \end{bmatrix} \tag{32}$$

$$A_9 = \begin{bmatrix} t_5^3 & t_5^2 & t_5 & 1 \\ 3t_5^2 & 2t_5 & 1 & 0 \\ 6t_5 & 2 & 0 & 0 \\ 0 & 0 & 0 & 1 \end{bmatrix} \tag{33}$$

$$x_1 = \begin{bmatrix} a_{13} & a_{12} & a_{11} & a_{10} \end{bmatrix}^T \tag{34}$$

$$x_2 = \begin{bmatrix} a_{24} & a_{23} & a_{22} & a_{21} & a_{20} \end{bmatrix}^T \tag{35}$$

$$x_3 = \begin{bmatrix} a_{35} & a_{34} & a_{33} & a_{32} & a_{31} & a_{30} \end{bmatrix}^T \tag{36}$$

$$x_4 = \begin{bmatrix} a_{44} & a_{43} & a_{42} & a_{41} & a_{40} \end{bmatrix}^T \tag{37}$$

$$x_5 = \begin{bmatrix} a_{53} & a_{52} & a_{51} & a_{50} \end{bmatrix}^T \tag{38}$$

$$B_1 = \begin{bmatrix} 0 & 0 & 0 & \theta_1 \end{bmatrix}^T \tag{39}$$

$$B_2 = \begin{bmatrix} 0 & 0 & 0 & 0 & 0 \end{bmatrix}^T \tag{40}$$

$$B_3 = \begin{bmatrix} 0 & \theta_2 & 0 & 0 & 0 & 0 \end{bmatrix}^T \tag{41}$$

$$B_4 = \begin{bmatrix} \theta_3 & 0 & 0 & 0 & \theta_4 \end{bmatrix}^T \tag{42}$$

$$B_5 = \begin{bmatrix} \theta_6 & 0 & 0 & \theta_5 \end{bmatrix}^T \tag{43}$$

Summarily, the combination coefficient matrix of multiple high-order polynomial mixed interpolation is:

$$x = A^{-1} * B \tag{44}$$

The coefficients of various high-order polynomial mixed interpolations under given time conditions and solutions for the five-segment multinomial mixed interpolation expressions in the discrete state can be obtained using the above matrix function relationship.

Under similar constraints, the same high-order polynomial was used for different combinations to establish 3-4-7-4-3 and 3-3-7-3-3 relationships for any joint variable in the excavator joint space.

The 3-4-7-4-3 polynomial interpolation expression of any joint variable in the excavator joint space was set as:

$$\begin{cases} h_1(t) = a_{13}t^3 + a_{12}t^2 + a_{11}t + a_{10} \\ h_2(t) = a_{24}t^4 + a_{23}t^3 + a_{22}t^2 + a_{21}t + a_{20} \\ h_3(t) = a_{37}t^7 + a_{36}t^6 + a_{35}t^5 + a_{34}t^4 + a_{33}t^3 + a_{32}t^2 + a_{31}t + a_{30} \\ h_4(t) = a_{44}t^4 + a_{43}t^3 + a_{42}t^2 + a_{41}t + a_{40} \\ h_5(t) = a_{53}t^3 + a_{52}t^2 + a_{51}t + a_{50} \end{cases} \tag{45}$$

The 3-3-7-3-3 polynomial interpolation expression of any joint variable in the excavator joint space was set as:

$$\begin{cases} h_1(t) = a_{13}t^3 + a_{12}t^2 + a_{11}t + a_{10} \\ h_2(t) = a_{23}t^3 + a_{22}t^2 + a_{21}t + a_{20} \\ h_3(t) = a_{37}t^7 + a_{36}t^6 + a_{35}t^5 + a_{34}t^4 + a_{33}t^3 + a_{32}t^2 + a_{31}t + a_{30} \\ h_4(t) = a_{43}t^3 + a_{42}t^2 + a_{41}t + a_{40} \\ h_5(t) = a_{53}t^3 + a_{52}t^2 + a_{51}t + a_{50} \end{cases} \tag{46}$$

The uniformity of each excavation trajectory time was set to ensure the continuity of the excavator during operation and analyze the continuity of angular velocity, angular acceleration, and jerk change rate under high-order mixed interpolation polynomial. Combined with the relationship function between the combination coefficient matrix of high-order polynomial mixed interpolation and the excavation time, the expressions of three different high-order polynomial mixed interpolations of excavator boom, bucket rod, and bucket were computed.

The interpolation expression of the variable order polynomial of excavator boom joint 3-4-5-4-3 is:

$$\begin{cases} \theta_1(t) = & -0.0289t^3 + 34.83(0 \le t \le 3) \\ \theta_2(t) = & -0.0401t^4 + 0.8941t^3 - 6.1415t^2 + 16.2591t + 19.6536(3 \le t \le 6) \\ \theta_3(t) = & 0.1026t^5 - 3.617t^4 + 49.8037t^3 - 335.52t^2 \\ & +1112.1576t - 1424.7404(6 \le t \le 9) \\ \theta_4(t) = & -0.4924t^4 + 20.4252t^3 - 312.8982t^2 + 2098.4066t - 5158.4896(9 \le t \le 12) \\ \theta_5(t) = & 0.3359t^3 - 15.1157t^2 + 226.738t - 1075.2404(12 \le t \le 15) \end{cases} \tag{47}$$

The interpolation expression of the variable order polynomial of excavator arm joint 3-4-5-4-3 is:

$$\begin{cases} \theta_1(t) = & -0.3778t^3 - 40.3200(0 \le t \le 3) \\ \theta_2(t) = & -0.479t^4 + 8.8939t^3 - 57.5791t^2 + 146.8713t - 174.2583(3 \le t \le 6) \\ \theta_3(t) = & -0.1248t^5 + 4.845t^4 - 73.954t^3 + 553.2672t^2 \\ & -2026.9432t + 2843.8488(6 \le t \le 9) \\ \theta_4(t) = & 0.096t^4 - 4.0758t^3 + 64.7834t^2 - 460.6106t + 1161.7122(9 \le t \le 12) \\ \theta_5(t) = & -0.1111t^3 + 4.9996t^2 - 74.9952t + 282.8508(12 \le t \le 15) \end{cases} \tag{48}$$

The interpolation expression of the variable order polynomial of excavator bucket joint 3-4-5-4-3 is:

$$\begin{cases} \theta_1(t) = & -0.0485t^3 - 56.16(0 \le t \le 3) \\ \theta_2(t) = & -0.0941t^4 + 1.6773t^3 - 10.451t^2 + 26.2717t - 79.8911(3 \le t \le 6) \\ \theta_3(t) = & -0.0441t^5 + 1.6627t^4 - 24.6094t^3 + 178.4991t^2 \\ & -634.2684t + 825.1856(6 \le t \le 9) \\ \theta_4(t) = & 0.0719t^4 - 3.0602t^3 + 48.314t^2 - 335.3158t + 803.4181(9 \le t \le 12) \\ \theta_5(t) = & -0.03t^3 + 1.35t^2 - 20.25t + 40.18(12 \le t \le 15) \end{cases} \tag{49}$$

The interpolation expression of the variable order polynomial of excavator boom joint 3-4-7-4-3 is:

$$\begin{cases} \theta_1(t) = -0.0289t^3 + 34.83(0 \le t \le 3) \\ \theta_2(t) = -0.0339t^4 + 0.8011t^3 - 5.6393t^2 + 15.0873t + 20.658(3 \le t \le 6) \\ \theta_3(t) = -0.0192t^7 + 0.9878t^6 - 21.4972t^5 + 256.6221t^4 - 1816.335t^3 \\ \quad +7631.5173t^2 - 17645.252t + 17370.4792(6 \le t \le 9) \\ \theta_4(t) = -0.4654t^4 + 19.2108t^3 - 292.5042t^2 + 1946.9546t - 4739.185(9 \le t \le 12) \\ \theta_5(t) = 0.3359t^3 - 15.1157t^2 + 226.738t - 1075.2402(12 \le t \le 15) \end{cases} \tag{50}$$

The interpolation expression of the variable order polynomial of excavator arm joint 3-4-7-4-3 is:

$$\begin{cases} \theta_1(t) = -0.3778t^3 - 40.32(0 \le t \le 3) \\ \theta_2(t) = -0.4544t^4 + 8.5248t^3 - 55.5856t^2 + 142.2192t - 170.2704(3 \le t \le 6) \\ \theta_3(t) = 0.0236t^7 - 1.2535t^6 + 28.1951t^5 - 347.8334t^4 + 2540.0092t^3 \\ \quad -10975.6006t^2 + 25989.0202t - 26096.2716(6 \le t \le 9) \\ \theta_4(t) = 0.0952t^4 - 4.0393t^3 + 64.1637t^2 - 455.9697t + 1148.7801(9 \le t \le 12) \\ \theta_5(t) = -0.1111t^3 + 4.9996t^2 - 74.9952t + 282.8508(12 \le t \le 15) \end{cases} \tag{51}$$

The interpolation expression of the variable order polynomial of excavator bucket joint 3-4-7-4-3 is:

$$\begin{cases} \theta_1(t) = -0.0485t^3 - 56.16(0 \le t \le 3) \\ \theta_2(t) = -0.0891t^4 + 1.6024t^3 - 10.0469t^2 + 25.3294t - 79.0838(3 \le t \le 6) \\ \theta_3(t) = 0.008t^7 - 0.4206t^6 + 9.3628t^5 - 114.3291t^4 + 826.8666t^3 \\ \quad -3542.5137t^2 + 8329.5925t - 8358.991(6 \le t \le 9) \\ \theta_4(t) = 0.0683t^4 - 2.8978t^3 + 45.5806t^2 - 314.982t + 747.0493(9 \le t \le 12) \\ \theta_5(t) = -0.03t^3 + 1.35t^2 - 20.25t + 40.18(12 \le t \le 15) \end{cases} \tag{52}$$

The interpolation expression of the variable order polynomial of excavator boom joint 3-3-7-3-3 is:

$$\begin{cases} \theta_1(t) = -0.0289t^3 + 34.83(0 \le t \le 3) \\ \theta_2(t) = 0.2926t^3 - 2.8934t^2 + 8.6802t + 26.1498(3 \le t \le 6) \\ \theta_3(t) = -0.4188t^7 + 21.6613t^6 - 476.2186t^5 + 5768.8072t^4 - 41592.4322t^3 \\ \quad +178528.6665t^2 - 422561.5364t + 425649.136(6 \le t \le 9) \\ \theta_4(t) = -1.7326t^3 + 59.3502t^2 - 666.8518t + 2499.1154(9 \le t \le 12) \\ \theta_5(t) = 0.3359t^3 - 15.1157t^2 + 226.738t - 1075.2404(12 \le t \le 15) \end{cases} \tag{53}$$

The interpolation expression of the variable order polynomial of excavator arm joint 3-3-7-3-3 is:

$$\begin{cases} \theta_1(t) = -0.3778t^3 - 40.32(0 \leq t \leq 3) \\ \theta_2(t) = 0.2444t^3 - 7.7988t^2 + 78.5892t - 331.4976(3 \leq t \leq 6) \\ \theta_3(t) = 0.5324t^7 - 28.1853t^6 + 634.5712t^5 - 7873.7836t^4 + 58137.7153t^3 \\ \qquad -255419.9882t^2 + 618245.5764t - 636192.6432(6 \leq t \leq 9) \\ \theta_4(t) = 1.4478t^3 - 48.8773t^2 + 537.876t - 2036.2389(9 \leq t \leq 12) \\ \theta_5(t) = -0.1111t^3 + 4.9996t^2 - 74.9952t + 282.8508(12 \leq t \leq 15) \end{cases} \tag{54}$$

The interpolation expression of the variable order polynomial of excavator bucket joint 3-3-7-3-3 is:

$$\begin{cases} \theta_1(t) = -0.0485t^3 - 56.16(0 \leq t \leq 3) \\ \theta_2(t) = 0.2659t^3 - 2.8298t^2 + 8.4895t - 64.6496(3 \leq t \leq 6) \\ \theta_3(t) = 0.1537t^7 - 8.0827t^6 + 180.7501t^5 - 2227.6826t^4 + 16340.0443t^3 \\ \qquad -71330.5223t^2 + 171611.1124t - 175631.4304(6 \leq t \leq 9) \\ \theta_4(t) = 0.1756t^3 - 6.0512t^2 + 68.5608t - 315.0524(9 \leq t \leq 12) \\ \theta_5(t) = -0.03t^3 + 1.35t^2 - 20.25t + 40.18(12 \leq t \leq 15) \end{cases} \tag{55}$$

3.3. Trajectory Simulation

To compare the advantages and disadvantages of three different higher-order mixed polynomial interpolation strategies, discrete points of the excavator trajectory in Figure 8 were selected, and the joint variables of the excavator manipulator computed at each discrete point based on the inverse kinematics solution formula of the excavator's joints (4); According to the digging characteristics of the excavator, the zero points of the angular velocity and acceleration of the starting point, as well as the ending point of each joint, were excavated to facilitate the analysis and setting of the time unity of each digging trajectory.

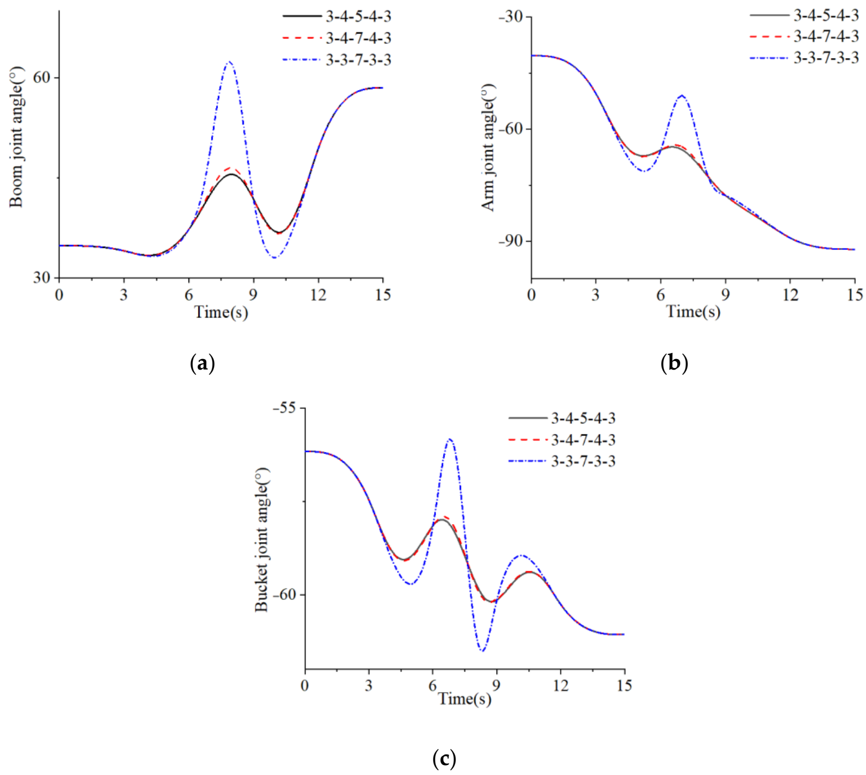

Figure 8. Joint angle curves by three different higher-order mixed polynomials: (**a**) boom, (**b**) arm, and (**c**) bucket.

Utilizing the angle values of each joint of the excavator in Table 2, in conjunction with the function expressions of three different higher-order mixed polynomial interpolations solved under the constraints of Formulas (17)~(20), the law of the change in the angle, angular velocity, and angular acceleration of each joint of the excavator with the mining time under the three interpolation methods was simulated and analyzed in Matlab R2023a(Free MATLAB Trial). Figures 8–10 exhibit the angular curves, velocity, and acceleration of each joint of the excavator with time.

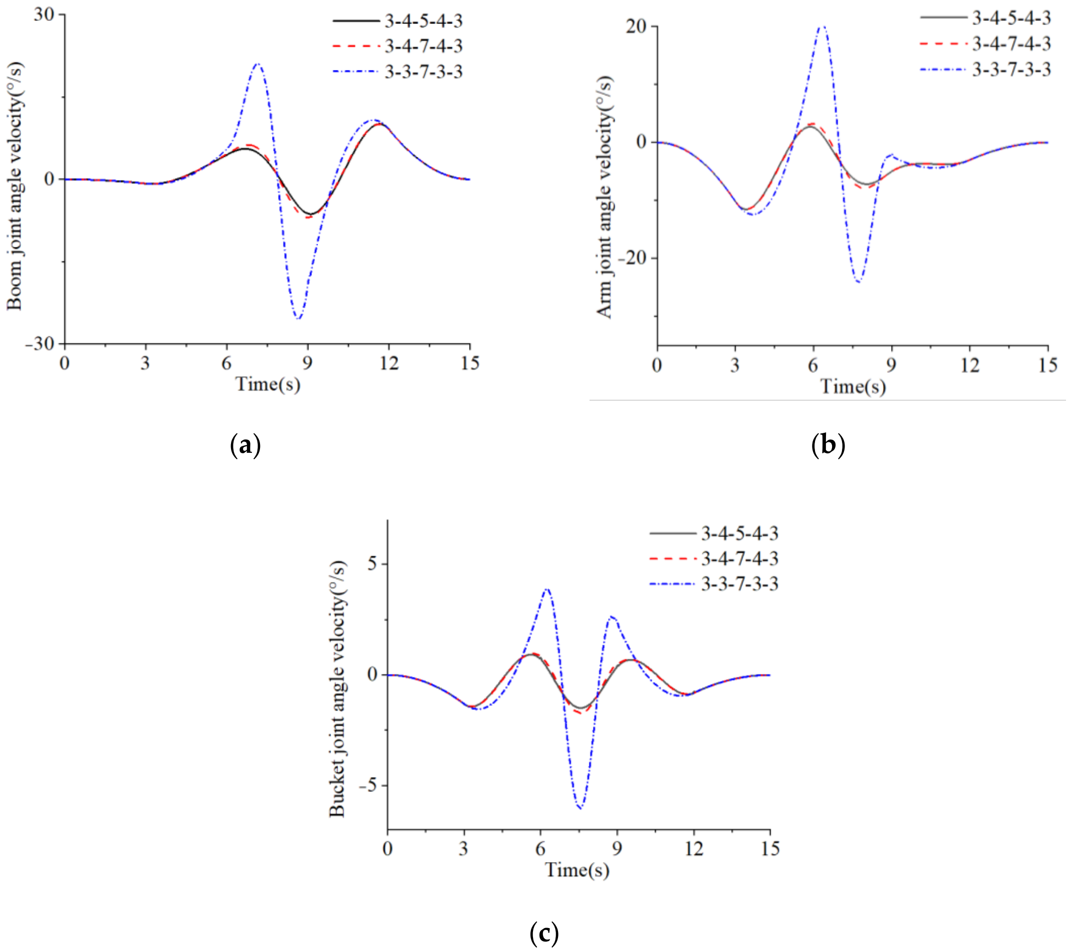

Figure 9. Joint angular velocity curves by three different higher-order mixed polynomials: (**a**) boom, (**b**) arm, and (**c**) bucket.

As presented above, the angle curves of each joint of the excavator pass through the selected discrete angle points and maintain good continuity in three different high-order mixed polynomial interpolation plans. In contrast to the three hybrid polynomial interpolation strategies, the 3-3-7-3-3 interpolation strategy induces a substantial fluctuation of the angle variables of each joint of the excavator, which is not favorable for the smoothness of the excavator operation.

As presented, the angular velocity of each joint of the excavator exhibits temporal variations, with an adequately continuous and smooth curve. However, the 3-3-7-3-3 interpolation strategy's angular velocity curve demonstrates significant fluctuations, impeding the stability of each joint trajectory during operation. In contrast, under the 3-4-5-4-3 interpolation strategy, the maximum angular velocity of the boom, stick angle, and bucket was reduced by 68.33%, 48.34%, and 56.17%, respectively, when compared with the 3-3-7-3-3 interpolation strategy. The angular velocity change curve under both the 3-4-5-4-3 and 3-4-7-4-3 interpolation strategies demonstrates minimal fluctuations. Moreover, the angular velocity variation curve under these two different interpolation strategies exhibits similarities, mainly due to the polynomial interpolation used in the third digging path trajectory, which varies between the two strategies.

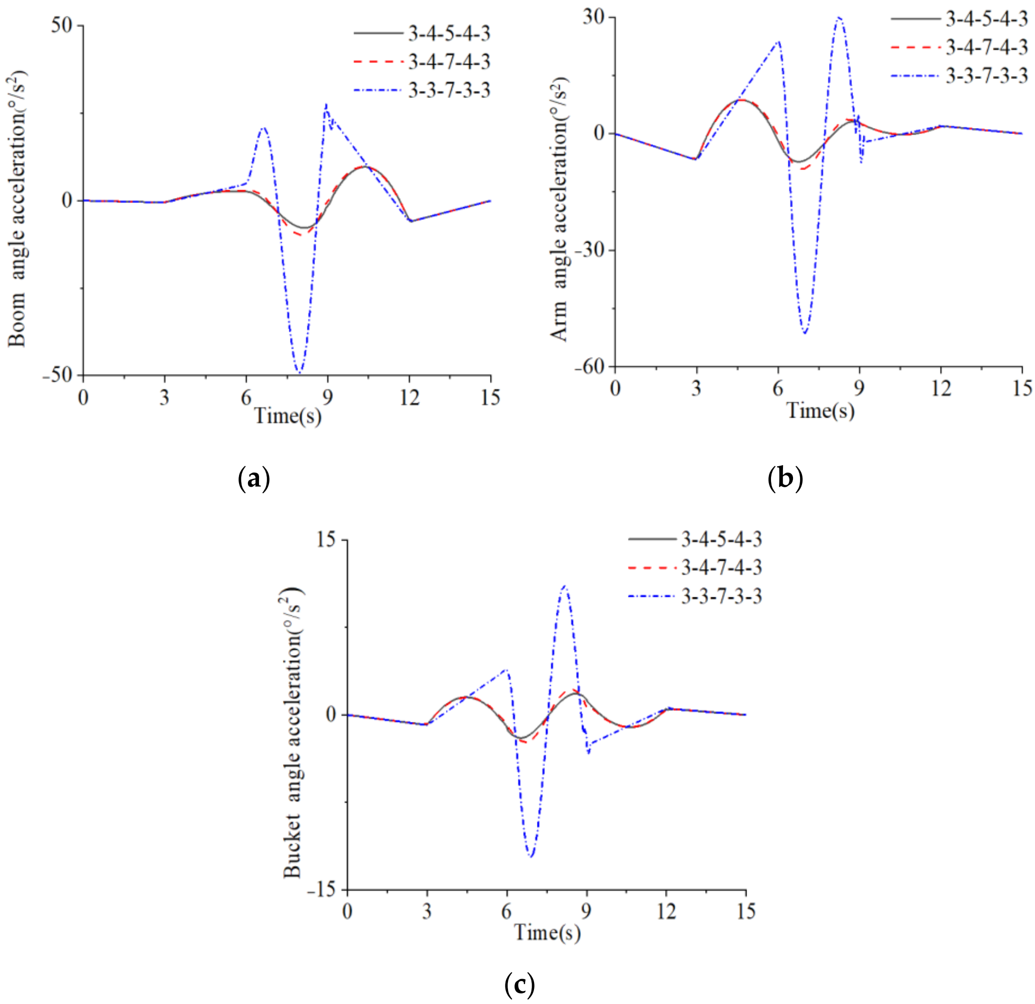

Figure 10. Joint angular acceleration curves by three different higher-order mixed polynomials: (**a**) boom, (**b**) arm, and (**c**) bucket.

Therefore, the curve of angular acceleration change exhibits a significant mutation in the case of the 3-3-7-3-3 interpolation strategy. Conversely, the angular acceleration curves for the 3-4-5-4-3 and 3-4-7-4-3 interpolation strategies display negligible changes. In contrast to the 3-3-7-3-3 interpolation strategy, the 3-4-5-4-3 strategy reduces the maximum angular acceleration of the boom by 82.01%, the maximum angular acceleration of the bucket rod by 89.54%, and the maximum angular acceleration of the bucket by 85.869%. The abrupt change and large fluctuation of the acceleration values cause the vibration and impact of the excavator's arm, thereby decreasing the service life of the excavator structure.

In conclusion, an analysis of three different high-order mixed polynomial interpolation strategies was conducted from the angle, angular velocity, and angular acceleration continuity, smoothness, and volatility of each joint of the excavator. As a result, the excavator trajectory planning under the 3-4-5-4-3 interpolation strategy operates smoothly, reduces the flexible impact during the joint operation, and enhances the stability and precision of the trajectory operation.

4. Experimental Research

To analyze the reliability of higher-order mixed interpolation polynomial trajectory planning, the 3-4-5-4-3 interpolation trajectory of each excavator's joint in Figure 8 was substituted into Formulas (6), (8), and (13), and the angles of each excavator joint space under the interpolation strategy were converted into the displacement variables of the hydraulic actuator in the drive space.

Furthermore, the single-bucket excavator experimental platform was established, and the displacement of each hydraulic actuator in the drive space was considered the target curve. The accuracy of the proposed high-order mixed interpolation polynomial trajectory planning was confirmed through experimental analysis.

4.1. Excavator Experimental Platform

The single-bucket excavator hydraulic system was composed of a hydraulic pump, independent control valve group, and hydraulic actuator. The hydraulic pump mainly serves as the hydraulic source for the system to supply the operation of each actuator. The hydraulic valve group primarily controls the movement direction of the actuator; and the hydraulic actuator was leveraged to push the connected mechanical structure to enable the excavator manipulator to operate under various working conditions.

This study focuses on the closed-loop control of the hydraulic actuator of an excavator. A line displacement sensor, which offers a linear accuracy of 0.1% FS, was employed for real-time detection of the boom, stick, and bucket cylinder displacement. The displacement values were fed back to the controller, which calculated the deviation from the target parameters and adjusted the spool opening of the load port of the independent control valve group accordingly. This facilitated control over the hydraulic actuator displacement variable and enabled closed-loop displacement control of the hydraulic actuator. The excavator experimental platform is shown in Figure 11.

Figure 11. Excavator experimental platform.

4.2. Experimental Analysis

On the excavator experimental platform, the closed-loop experimental research on the displacement of the excavator hydraulic actuator converted by the higher-order mixed interpolation polynomial trajectory planning was conducted. The difference curve between the target displacement and the experimental displacement of the hydraulic actuator is shown in Figure 12.

Figure 12 indicates that in the experimental study of the displacement difference variables of each actuator of the excavator, the system control accuracy and dynamic response are fast, which can ensure the continuity and stability of the operation of the actuator. The experimental displacement of the hydraulic actuator exhibits a small error with the target displacement, which meets the actual working conditions of the excavator manipulator and verifies the effectiveness of the proposed high-order hybrid polynomial interpolation strategy.

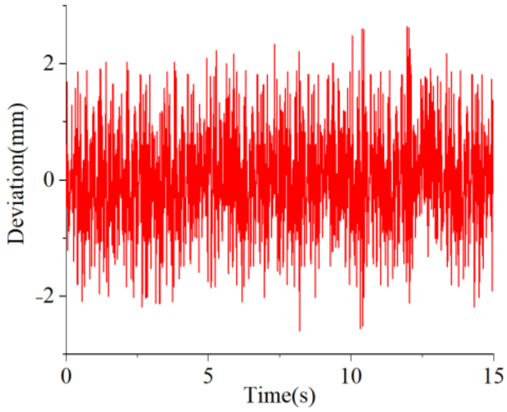

(**a**)

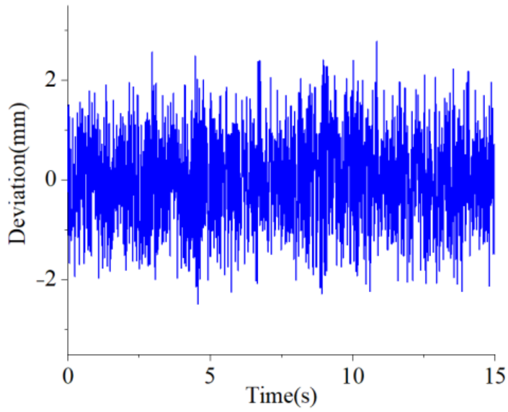

(**b**)

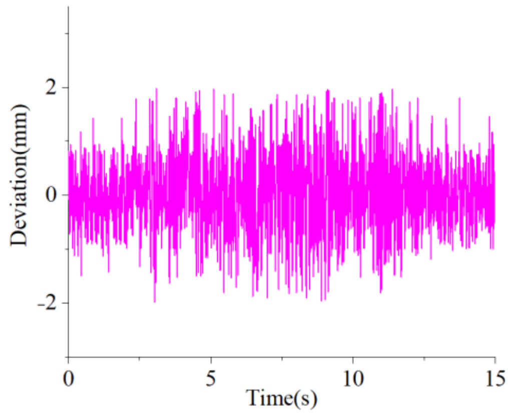

(**c**)

Figure 12. Displacement error experimental curve of hydraulic actuator: (**a**) boom, (**b**) arm, and (**c**) bucket.

5. Conclusions

This paper proposed a trajectory planning strategy for an excavator, utilizing high-order mixed polynomial interpolation. Three distinct interpolation strategies (3-4-5-4-3, 3-4-7-4-3, and 3-3-7-3-3-3) were proposed to ensure continuity of the angle, angular velocity, and angular acceleration of the trajectory. This study focused on a single-bucket excavator and establishes a kinematics model to analyze the reachable space range of the tooth tip trajectory. Additionally, the mapping relationship between the joint space and driving space was solved. Next, this study selected a typical mining target trajectory and proposed the continuity requirements for velocity, acceleration, and jerk during trajectory operation. The three different high-order mixed polynomial interpolation strategies were then analyzed. After comparing the three interpolation strategies, it was found that the 3-4-5-4-3 strategy resulted in a reduction in the maximum angular velocity of the boom to $-25.07382°/s$, the maximum angular velocity of the stick angle to $-15.30593°/s$, and the maximum angular velocity of the bucket to $-13.88113°/s$. Additionally, this strategy reduced the maximum angular acceleration of the boom to $-23.7731°/s^2$, the maximum angular acceleration of the stick to $-6.89293°/s^2$, and the maximum angular acceleration of the bucket to $-10.89442°/s^2$. Experimental analysis was conducted to study the trajectory tracking of the optimal high-order mixed polynomial interpolation strategy. The results indicate the excavator tooth tip trajectory is continuous, stable, and accurate during operation.

The present results are of great significance for the excavator to independently plan the excavation trajectory. The use of mixed-order polynomial interpolation makes the excavation trajectory continuous and stable, reduces the mutation effect, the joint flexible impact, improves the service life of the mechanical structure body, and accurately complete the requirements of the excavation conditions.

Author Contributions: Conceptualization, R.G. and Y.G.; methodology, Y.G. and J.Z.; software, J.Y. and Q.G.; formal analysis, J.Y.; data curation, Q.G.; writing—original draft preparation, J.Y.; writing—review and editing, J.Y. and R.G.; supervision, Y.G.; funding acquisition, R.G. All authors have read and agreed to the published version of the manuscript.

Funding: This research was funded by the National Natural Science Foundation of China (12173054, 52075469).

Institutional Review Board Statement: Not applicable.

Informed Consent Statement: Not applicable.

Data Availability Statement: Not applicable.

Conflicts of Interest: The authors declare that they have no conflict of interest.

References

1. Li, Y.; Fan, R.; Yang, L.; Zhao, B.; Quan, L. Research Status and Development Trend of Intelligent Excavators. *J. Mech. Eng.* **2020**, *56*, 165–178.
2. Eraliev, O.; Lee, K.; Shin, D.; Lee, C. Sensing, perception, decision, planning and action of autonomous excavators. *Autom. Constr.* **2022**, *141*, 104428. [CrossRef]
3. Zhang, L.; Zhao, J.; Long, P.; Wang, L.; Qin, L.; Lu, F.; Song, X.; Manocha, D. An autonomous excavator system for material loading tasks. *Sci. Robot.* **2021**, *6*, 3164–3175. [CrossRef] [PubMed]
4. Yuan, C.; Li, S.; Cai, H. Vision-Based Excavator Detection and Tracking Using Hybrid Kinematic Shapes and Key Nodes. *J. Comput. Civ. Eng.* **2017**, *31*, 4016038.1–4016038.16. [CrossRef]
5. Yoo, H.; Young-Suk, K. Development of a 3D local terrain modeling system of intelligent excavation robot. *KSCE J. Civ. Eng.* **2016**, *21*, 565–578. [CrossRef]
6. Jud, D.; Leemann, P.; Kerscher, S.; Hutter, M. Autonomous free-form trenching using a walking excavator. *IEEE Robot. Autom. Lett.* **2019**, *4*, 3208–3215. [CrossRef]
7. Quang, H.; Lee, Q.; Yang, S. Remote control of excavator using head tracking and flexible monitoring method. *Autom. Constr.* **2017**, *81*, 99–111.
8. Li, G.; Zhang, Q.; Xiao, M. Fault Diagnosis Research of Hydraulic Excavator Based on Fault Tree and Fuzzy Neural Network. *Appl. Mech. Mater.* **2013**, *303*, 1350–1356. [CrossRef]
9. Li, G.; Qing, W. Hydraulic Fault Diagnosis Expert System of Excavator Based on Fault Tree. *Adv. Mater. Res.* **2011**, *228*, 439–446. [CrossRef]
10. Young, B.; Junhyoung, H.; Hyuk, K.; Pan, Y.; Fc, P. Dynamically optimal trajectories for earthmoving excavators. *Autom. Constr.* **2013**, *35*, 568–578.
11. Tremblay, L.; Arsenault, M.; Zeinali, M. Development of a trajectory planning algorithm for a 4-DoF rockbreaker based on hydraulic flow rate limits. *Trans. Can. Soc. Mech. Eng.* **2020**, *44*, 501–510. [CrossRef]
12. Jud, D.; Hottiger, G.; Leemann, P.; Hutter, M. Planning and Control for Autonomous Excavation. *IEEE Robot. Autom. Lett.* **2017**, *2*, 2151–2158. [CrossRef]
13. Fan, R.; Li, Y.; Yang, L. Multiobjective trajectory optimization of intelligent electro-hydraulic shovel. *Front. Mech. Eng.* **2022**, *17*, 1–24. [CrossRef]
14. Zhang, B.; Wang, S.; Liu, Y.; Yang, H. Research on Trajectory Planning and Autodig of Hydraulic Excavator. *Math. Probl. Eng. Theory Methods Appl.* **2017**, *2017*, 1–10. [CrossRef]
15. Luo, L.; Yuan, C.; Yan, R.; Yuan, Q.; Wu, J.; Shin, K.; Han, C. Trajectory planning for energy minimization of industry robotic manipulators using the Lagrange interpolation method. *Int. J. Precis. Eng. Manuf.* **2015**, *16*, 911–917. [CrossRef]
16. Zhang, Y.; Sun, Z.; Sun, Q.; Wang, Y.; Li, X.; Yang, J. Time-jerk optimal trajectory planning of hydraulic robotic excavator. *Adv. Mech. Eng.* **2021**, *13*, 1–13. [CrossRef]
17. Vu, N.; Tran, N. Path planning for excavator arm: Fuzzy logic control approach. *J. Robot.* **2020**, *2020*, 8893260. [CrossRef]
18. Wang, X.; Sun, W.; Li, E.; Song, X. Energy-minimum optimization of the intelligent excavating process for large cable shovel through trajectory planning. *Struct. Multidiscip. Optim.* **2018**, *58*, 2219–2237. [CrossRef]
19. Zou, Z.; Chen, J.; Pang, X. Task space-based dynamic trajectory planning for digging process of a hydraulic excavator with the integration of soil–bucket interaction. *Proc. Inst. Mech. Eng. Part K J. Multi-Body Dyn.* **2019**, *233*, 598–616. [CrossRef]
20. Zhao, J.; Hu, Y.; Liu, C.; Tian, M.; Xia, X. Spline-Based Optimal Trajectory Generation for Autonomous Excavator. *Machines* **2022**, *10*, 538. [CrossRef]
21. Im, Y.; Shin, D.; Hwang, S. Development of Trajectory Tracking Controller for Automatic Excavator System. *J. Drive Control.* **2019**, *16*, 109–113.

22. Bi, Q.; Wang, G.; Wang, Y.; Yao, Z.; Robert, H. Digging Trajectory Optimization for Cable Shovel Robotic Excavation based on a Multi-Objective Genetic Algorithm. *Energies* **2020**, *13*, 3118. [CrossRef]
23. Zhang, T.; Fu, T.; Song, X.; Qu, F. Multi-objective excavation trajectory optimization for unmanned electric shovels based on pseudospectral method. *Autom. Constr.* **2022**, *136*, 104176. [CrossRef]
24. Yuasa, T.; Masato, I.; Satoshi, O. An optimal design methodology for the trajectory of hydraulic excavators based on genetic algorithm. *J. Robot. Mechatron.* **2021**, *33*, 1248–1254. [CrossRef]
25. Yang, Y.; Long, P.; Song, X.; Pan, J.; Zhang, L. Optimization-Based Framework for Excavation Trajectory Generation. *IEEE Robot. Autom. Lett.* **2021**, *6*, 1479–1486. [CrossRef]
26. Sun, Z.; Zhang, Y.; Li, H.; Sun, Q.; Wang, Y. Time Optimal Trajectory Planning of Excavator. *J. Mech. Eng.* **2019**, *55*, 166–174. [CrossRef]
27. Li, H.; Lin, Z.; Du, J.; Chen, Z. Piecewise Polynomial with Variable Order in Trajectory Planning for Autonomous Mining. *Trans. Chin. Soc. Agric. Mach.* **2016**, *47*, 319–325.
28. Wonohadidjojo, D.; Kothapalli, G.; Hassan, M. Displacement and vibration reduction system in hydraulic excavator. *Emir. J. Eng. Res.* **2014**, *19*, 1–10.
29. Klanfar, M.; Herceg, V.; Kuhinek, D.; Sekulić, K. Construction and testing of the measurement system for excavator productivity. *Rud. Geološko-Naft. Zb.* **2019**, *34*, 51–58. [CrossRef]
30. Curduman, L.; Nastac, S.; Debeleac, C. On active control of transitory regimes within the driving system of a single bucket excavating equipment for the bank-sloping and differential excavation processes. In Proceedings of the 23rd International Congress on Sound & Vibration (ICSV23), Athens, Greece, 10–14 July 2016; p. 794.
31. Curduman, L.; Carmen, D.; Silviu, N. Analysis of working body track vibrations of a single bucket excavating equipment during the bank-sloping and differential excavation processes. In Proceedings of the 23rd International Congress on Sound & Vibration (ICSV23), Athens, Greece, 10–14 July 2016; p. 793.
32. Gurko, A.; Sergiyenko, O.; Hipólito, J.; Kirichenko, I.; Tyrsa, V.; Lopez, J. Guaranteed control of a robotic excavator during digging process. In Proceedings of the 2015 12th International Conference on Informatics in Control, Automation and Robotics (ICINCO), Alsace, France, 21–23 July 2015; Volume 2, pp. 52–59.
33. Jin, K.; Park, T.; Lee, H. A control method to suppress the swing vibration of a hybrid excavator using sliding mode approach. Proceedings of the institution of mechanical engineers. *Part C J. Mech. Eng. Sci.* **2012**, *226*, 1237–1253. [CrossRef]